Bioorganic & Medicinal Chemistry 20 (2012) 2889–2896

Contents lists available at SciVerse ScienceDirect

Bioorganic & Medicinal Chemistry

journal homepage: www.elsevier.com/locate/bmc

Radiofluorinated histamine H_3 receptor antagonist as a potential probe for in vivo PET imaging: Radiosynthesis and pharmacological evaluation

Svetlana V. Selivanova [a,*], Michael Honer [a], Francine Combe [a], Kathleen Isensee [b], Holger Stark [b], Stefanie D. Krämer [a], P. August Schubiger [a], Simon M. Ametamey [a]

[a] Center for Radiopharmaceutical Sciences, Department of Chemistry and Applied Biosciences, ETH Zurich (Swiss Federal Institute of Technology), Wolfgang-Pauli-Strasse 10, CH-8093 Zurich, Switzerland

[b] Institute of Pharmaceutical Chemistry, ZAFES/LiFF/OSF, Johann Wolfgang Goethe University, Biozentrum Max-von-Laue-Strasse 9, 60348 Frankfurt-am-Main, Germany

ARTICLE INFO

Article history:
Received 16 December 2011
Revised 5 March 2012
Accepted 9 March 2012
Available online 17 March 2012

Keywords:
Histamine H_3 receptor
H_3R
PET imaging
Neurological disorders
CNS

ABSTRACT

The histamine H_3 receptor (H_3R) plays a role in cognition and memory processes and is implicated in different neurological disorders, including Alzheimer's disease, schizophrenia, and narcolepsy. In vivo studies of the H_3R occupancy using a radiolabeled PET tracer would be very useful for CNS drug discovery and development. We report here the radiosynthesis, in vitro and in vivo evaluation of a novel ^{18}F-labeled high-affinity H_3R antagonist ^{18}F-ST889. The radiosynthesis was accomplished via nucleophilic substitution of the mesylate leaving group with a radiochemical yield of 8–20%, radiochemical purity >99%, and specific radioactivity >65 GBq/μmol. ^{18}F-ST889 exhibited high in vivo stability and rather low lipophilicity ($\log D_{7.4} = 0.35 \pm 0.09$). In vitro autoradiography showed specific binding in H_3R-rich brain regions such as striatum and cortex. However, in vivo PET imaging of the rat brain with ^{18}F-ST889 was not successful. Possible reasons are discussed.

1. Introduction

Histamine receptors are G-protein coupled receptors (GPCRs). They exist in four different subtypes named H_1R to H_4R. H_1R and H_2R are targets for anti-allergy and anti-ulcer medications, respectively.[1] H_4R is claimed to be acting in inflammation and immune response.[2,3] H_3R plays an important role in neuronal activities such as cognition and memory.[4] It is thought to be involved in different neurological disorders, including Alzheimer's disease,[5] attention-deficit/hyperactivity disorder,[5] narcolepsy,[6,7] epilepsy,[6] and schizophrenia[8] among others.[1,9] H_3R was first identified pharmacologically in 1983 as a mediator of histamine release.[10] It is accepted now that among other physiological functions H_3R regulates excretion of histamine and other important neurotransmitters, such as acetylcholine, noradrenalin, dopamine, and serotonin.[11–13] H_3R is located mainly in the central nervous system (CNS) and is scarce in the periphery. It is distributed in many brain areas, namely the cerebral cortex, striatum, hypothalamus, substantia nigra, accumbens nucleus, olfactory tubercle, caudate, and amygdala, as identified by autoradiography in rodents.[8,14,15]

In vivo studies of the distribution and density of H_3R in humans and quantification of the receptor occupancy would be useful for CNS drug discovery and development. Positron-emission tomography (PET) can offer such an opportunity. For this, special probes labeled with positron-emitting radionuclides have to be developed. These radiolabeled compounds must possess very high affinity (low nanomolar to subnanomolar range), high target selectivity and appropriate pharmacokinetics, including the capability to cross the blood–brain barrier (BBB). The main radioisotopes used in PET are carbon-11 (^{11}C) and fluorine-18 (^{18}F). ^{18}F has excellent physical characteristics, including a longer half-life, allowing for lengthier synthetic procedures and the possibility to deliver to centers, which do not have their own dedicated radiochemistry laboratories and a cyclotron.

Attempts to prepare PET tracers for H_3R started back in the 1990's (Fig. 1). Two imidazole derivatives were radiolabeled with ^{18}F and ^{11}C, giving ^{18}F-FUB-272 and ^{11}C-UCL-1829, respectively. Biodistribution studies with ^{18}F-FUB-272 showed poor brain uptake and high non-specific binding. Similarly, ^{11}C-UCL-1829 revealed low brain penetration and very high uptake in the lungs.[16] Radiofluorinated VUF 5000 was considered as a potential probe but

Abbreviations: H_3R, histamine H_3 receptor; CNS, central nervous system; GPCRs, G-protein coupled receptors; BBB, blood–brain barrier; CYP, cytochrome-P450; P-gp, P-glycoprotein; PET, positron emission tomography; EOB, end of bombardment; EOS, end of synthesis; HPLC, high-performance liquid chromatography; UPLC, ultra performance liquid chromatography; TLC, thin-layer chromatography; DMF, dimethylformamide; DMSO, dimethylsulfoxide; PBS, phosphate buffered saline; TFA, trifluoroacetic acid; HEPES, 4-(2-hydroxyethyl)-1-piperazineethanesulfonate; DMEM, Dulbecco's modified Eagle medium; MW, molar weight; MDR1, multidrug resistance protein 1; MDCK, Madin–Darby canine kidney.

* Corresponding author. Tel.: +41 44 633 60 94; fax: +41 44 633 13 67.
E-mail address: svetlana.selivanova@pharma.ethz.ch (S.V. Selivanova).

0968-0896/$ - see front matter © 2012 Elsevier Ltd. All rights reserved.
http://dx.doi.org/10.1016/j.bmc.2012.03.024

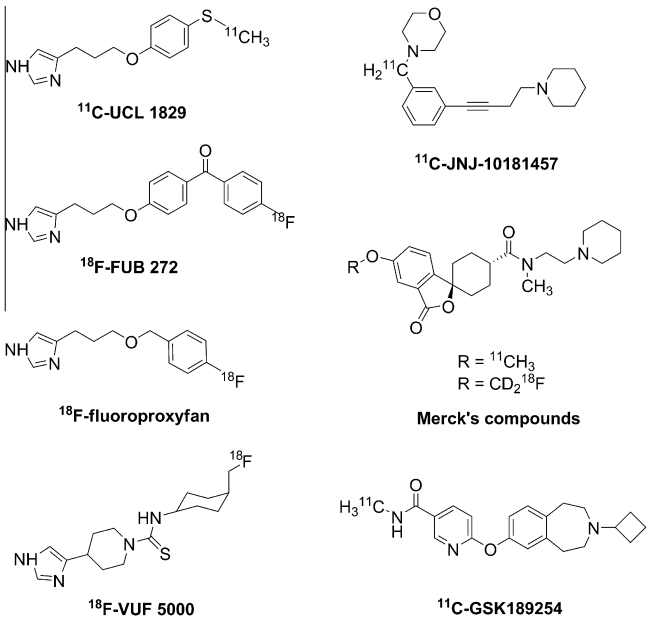

Figure 1. Previously attempted H_3R PET tracers.

showed low brain uptake in rats.[17,18] Synthetic steps were described for ^{18}F-fluoroproxyfan,[19] which shows saturable binding in vitro.[20] To our knowledge, no in vivo imaging was reported for this compound to date. The failure of the imidazole-containing compounds in general might be explained by their interaction with cytochrome-P450 (CYP) enzymes.[21] Ligands without imidazole moiety were also described. Selective H_3R ligand JNJ-10181457 labeled with ^{11}C had promising in vitro properties but failed in vivo due to high non-specific binding, which could not be blocked with H_3R antagonists.[22] More recently, a short report from Merck Laboratories described a carboxamide, which was labeled with either ^{11}C or ^{18}F and showed good in vivo binding and specificity.[23] In vivo PET studies in rhesus monkeys using either of these tracers proved that they could be used to measure receptor occupancy by H_3R inverse agonists.[24] However, the radiofluorinated carboxamide analogue was obtained in rather modest yields. Moreover, the reaction is multistep and involves distillation of a radiolabeled intermediate, which is not optimal for an eventual automation. ^{11}C-GSK189254 progressed to the first human PET study in healthy volunteers and was found to be promising in quantifying H_3R in humans.[25,26] Despite recent developments and progress of ^{11}C-labeled radioligands into clinical trials, there is still a need for potent and specific H_3R tracers labeled with a longer-lived ^{18}F.

Recently, a series of novel non-imidazole histamine H_3R antagonists were described,[27] based on the lead structure of JNJ-5207852[28,29] and FUB 880[30] (Fig. 2). These compounds possess high affinity and selectivity to H_3R in vitro. In vivo potency was found to be high after oral administration to mice. Compound ST889 (Fig. 2) was selected as a potential PET tracer candidate due to its high binding affinity (hH_3R K_i = 0.094 nM)[27] and amenability to ^{18}F-radiolabeling.

This paper describes the radiosynthesis, in vitro and in vivo evaluation of ^{18}F-ST889 as a potential PET probe for imaging H_3R.

2. Results and discussion

2.1. Chemistry and radiochemistry

The precursor for the radiolabeling and cold reference compound were synthesized as described previously.[27]

Radiosynthesis (Scheme 1) was performed in one step and optimized for solvent (acetonitrile, DMF, DMSO), reaction time (5–30 min), and temperature (90–140 °C). Acetonitrile was the preferred solvent giving higher yields. Heating up to 140 °C in DMF or DMSO did not offer any improvement. Precursor concentration in a range of 17–35 μmol/mL did not influence the reaction yield noticeably, thus lower concentration was used. It should be noted that precursor concentration of 10–12 μmol/mL gave considerably lower yields. Purification was accomplished by semi-preparative HPLC and the product was collected in a volume of 3–4 mL. The final formulation was performed using solid phase extraction: the product was concentrated on a Sep-Pak Light C18 cartridge and eluted with 0.5 mL ethanol. Dilution with 9.5 mL of phosphate buffered saline (PBS) resulted in a solution acceptable for in vivo biological applications. Calculated radiochemical yields based on the isolated product were 8–20% (decay-corrected to the end of bombardment (EOB), n = 12). Typically, 4.1–9.5 GBq (110–257 mCi) of ^{18}F-ST889 could be obtained within 100–110 min (including HPLC purification) starting from ~80–100 GBq (2.1–2.7 Ci) of ^{18}F-fluoride.

To prepare an ethanol-free formulation, the eluate from the Sep-Pak cartridge was evaporated at room temperature under reduced pressure and a stream of nitrogen and the residue was reconstituted in PBS. Analysis of the formulated solution showed that ^{18}F-ST889 partially decomposed during the evaporation procedure, most probably due to self-radiolysis. Two polar products of the decomposition were detected in addition to the parent compound. One, likely ^{18}F-fluoride, was eluting with the solvent front, followed by a second unidentified compound, which was present only in selected batches. The extent of radiolysis was dependent on the shelf time. Radiochemical purity of the formulated in PBS ^{18}F-ST889 decreased to 89% 30 min after formulation and declined further to 73% after 2 h. Radiolysis is a known phenomenon for many compounds with high specific radioactivity and activity concentration.[31] It can be often avoided by addition of ascorbic acid or sodium ascorbate to the ethanolic solution of the radioactive

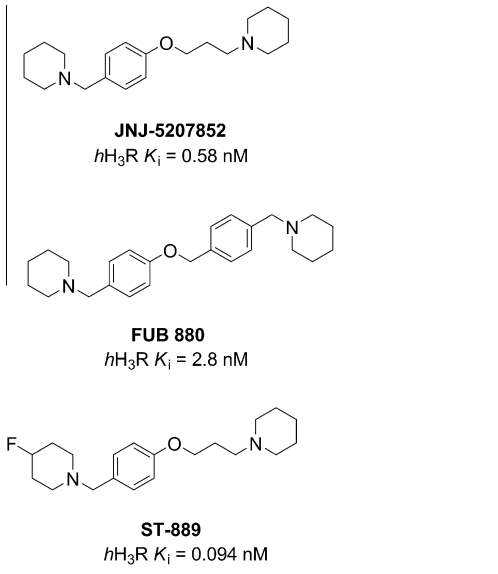

Figure 2. Non-imidazole H_3R antagonists.

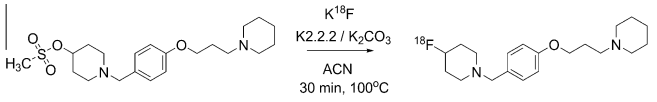

Scheme 1. Optimized radiolabeling conditions.

compound before evaporation. Addition of ascorbic acid (2 mg/mL, calculated for the final formulated solution volume) suppressed radiolysis and the final product was obtained in high activity concentration in ethanol-free aqueous solution. However, the ethanol containing formulation was used for biological studies described herein.

2.2. Quality control

Quality control of ^{18}F-ST889 was performed on an aliquot of the formulated radiopharmaceutical ready for injection using an analytical HPLC system. The pH of the clear colorless radiotracer solution was between 7 and 8. The product was >98% chemically and radiochemically pure and the formulation contained no precursor. The apparent specific activities were 65–100 GBq/μmol (1.7–2.7 Ci/μmol) at the end of synthesis (EOS). ^{18}F-ST889 was radiochemically stable in the solution for at least 4 h (confirmed by UPLC).

2.3. Binding affinity to rat H_3R

The K_i of the non-radioactive ST889 to human recombinant H_3R was reported to be 0.094 nM (pK_d 10.03).[27] To exclude significant species differences in the binding affinity of ^{18}F-ST889 between human and rat H_3R we determined the equilibrium dissociation constant K_d of ^{18}F-ST889 to native rat brain H_3R in a pilot experiment using rat whole brain homogenate. The estimated K_d value was 0.34 nM (pK_d 9.47) with maximum binding density (B_{max}) 930 fmol/mg protein. The B_{max} for the structurally similar JNJ-5207852 was reported to be 57 fmol/mg protein determined in rat cerebral cortex membranes.[29] Non-linear curve fitting and Scatchard plot analysis (Fig. 3) revealed one high affinity binding site. The estimated K_d of a low affinity interaction was $\geqslant$3 μM at B_{max} 220 pmol/mg protein. The high B_{max} value excludes specific binding to GPCRs in case of the low affinity interaction site. The binding potential (B_{max}/K_d) is about 40-fold higher for the high affinity binding, ruling out significant non-specific accumulation of the tracer in brain due to the low affinity binding. Only 55% of radioactivity was displaced by 10 μM (*R*)-α-methylhistamine while 10 μM cold ST889 displaced the ^{18}F-analogue (0.06 nM) completely (99.8%). The determined subnanomolar affinity to rat H_3R, although a slightly lower than to human H_3R, is suitable for PET imaging. A similar species-dependence was described for JNJ-5207852 with a pK_i of 9.24 to human H_3R and 8.90 to rat H_3R.[29]

2.4. Lipophilicity (log$D_{7.4}$)

In vivo H_3R targeting in the CNS requires good BBB passage of the ligand. The partition coefficient log*P* is often used to evaluate the ability of a drug to cross BBB. ^{18}F-ST889 is a base with two proton-accepting nitrogen atoms, which are protonated at physiological pH. For easily ionizable compounds the distribution coefficient log*D* at physiological pH 7.4 (log$D_{7.4}$) is used instead.[32]

Partitioning of ^{18}F-ST889 between octanol and phosphate buffer (pH 7.4) was determined using the shake-flask method.[33] The experimental log$D_{7.4}$ = 0.35 ± 0.09 was calculated from three independent determinations. This is a relatively low value but may still allow significant tracer concentration in the brain. Significant BBB permeation by passive diffusion is expected for compounds with log$D_{7.4}$ between 0 and 3.[32,34] However, many exceptions exist to this rule, including effective brain radiotracers.[35] There is also clear evidence that structurally similar JNJ-5207852 (Fig. 2) reaches high brain levels 60 min after subcutaneous administration in mice.[29] The addition of a fluoro-substituent to one of the piperidine rings may result in a minor loss in lipophilicity but is not expected to lessen brain accessibility drastically.[36,37]

2.5. In vitro metabolic stability in plasma and liver microsomes

The stability of ^{18}F-ST889 in plasma and liver microsomes was tested in vitro by incubating the radioligand with human or rodent plasma and liver microsomes at 37 °C. ^{18}F-ST889 showed good in vitro plasma stability without marked decomposition during the first 60 min. Minor defluorination occurred in human plasma after 90 min when ^{18}F-ST889 accounted for 98% of the total radioactivity in the sample with a decomposition degree still under 3% after 120 min.

^{18}F-ST889 was stable in human and rodent liver microsomes up to 120 min. The oxidative activity of the enzymes was confirmed with testosterone as positive control. After 90 min 60% of the initial testosterone was oxidized by human microsomes, while it was completely metabolized by rat microsomes.

2.6. In vitro autoradiography

In vitro autoradiography was carried out on horizontal rat brain slices with ^{18}F-ST889 alone or in the presence of 100 μM histamine. Tracer binding showed a heterogeneous distribution with the highest density in the striatum and cerebral cortex (Fig. 4). Moderate ^{18}F-ST889 binding was identified in hippocampus and

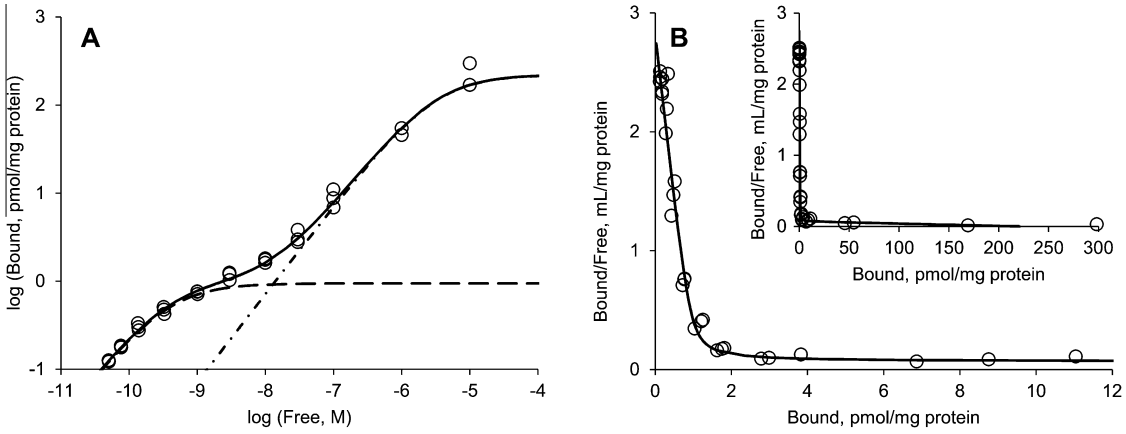

Figure 3. Binding affinity of ST889 to rat brain crude membranes. Rat brain crude membranes were incubated with 0.06 nM ^{18}F-ST889 and various concentrations of cold ST889. Bound ST889 (parameter B) and the molar concentration of free (unbound) ST889 were calculated from bound ^{18}F-ST889 and total ST889. A high and a low affinity binding site were identified by non-linear curve fitting (A). Continuous line: fit function shown in (Eq. 1); dashed line: contribution of high affinity binding site (fitted K_d 0.34 nM); dash-dot line: contribution of low affinity binding site (fitted K_d $\geqslant$3 μM). The results are displayed as a Scatchard plot with the fitted parameters (B). Expanded x-axis scale is in the insert.

thalamus, whereas binding in the cerebellum was clearly lower. This distribution of ligand binding is consistent with previously published data on the localization of H_3R in the rat brain.[9] Moreover, the tracer binding to striatum, cortex, hippocampus and thalamus was displaceable by co-incubation of ^{18}F-ST889 with 100 μM histamine. These results demonstrate the specificity of ^{18}F-ST889 for targeting H_3R in the rat brain in vitro.

2.7. Transport in P-glycoprotein-transfected cells in vitro

Besides low passive permeation across the brain capillary endothelium, efflux by P-glycoprotein (P-gp) in the luminal plasma membrane of the brain endothelial cells is another major obstacle for many compounds, in particular at tracer concentration.

In vivo P-gp susceptibility of bases with MW >250 and number of N and O atoms <4, to which category ^{18}F-ST889 belongs, is hardly predictable.[38] We investigated the passive permeation across a tight cell layer and possible efflux of ^{18}F-ST889 by P-gp with MDR1-transfected MDCK cells ($n = 6$ from 2 independent experiments). In this assay, P-gp transport of a substrate would result in a higher apparent permeability (P_{app}) coefficient from basal to apical (B→A) than from apical to basal (A→B).[39] The P_{app} A→B of ^{18}F-ST889 was $(1.6 \pm 0.7) \times 10^{-7}$ cm/s and P_{app} B→A was $(1.2 \pm 0.7) \times 10^{-7}$ cm/s, resulting in a ratio B→A/A→B of 0.8, indicating that ^{18}F-ST889 is not a substrate for human P-gp. Similar values were obtained in the presence of 10 μM elacridar, a specific P-gp inhibitor, and with the parent cell line MDCK (data not shown). Therefore, no efflux of ^{18}F-ST889 by P-gp is expected at the BBB of humans. However, differences in P-gp-efflux may exist between species, which was shown previously by transport experiments with MDR1 (human) and mdr1a (mouse) transfected epithelial cells.[40] P_{app} values of the P-gp substrate ^{3}H-vinblastine in the parallel experiment using the same MDCK-MDR1 cultures were $(2.2 \pm 1.4) \times 10^{-7}$ cm/s A→B and $(32.4 \pm 9.6) \times 10^{-7}$ cm/s B→A, with a ratio B→A/A→B of 15, confirming P-gp functionality.

When 100 μM verapamil was added to the apical compartment, P_{app} A→B for ^{18}F-ST889 increased to $(30.3 \pm 10.8) \times 10^{-7}$ cm/s, while P_{app} B→A was hardly affected $(1.9 \pm 0.7) \times 10^{-7}$ cm/s. The effect on ^{18}F-ST889 permeation was not seen at 10 μM verapamil, excluding any specific effect as well as an increase in barrier permeation under non-toxic verapamil doses to rats in vivo.

Although ^{18}F-ST889 is not a substrate for P-gp transport, BBB permeation may be at the limit for significant brain uptake as concluded from the relatively low P_{app} A→B and $\log D_{7.4}$ values. The extent of plasma protein binding and receptor density in the brain may have high impact on the final radiotracer accumulation level.

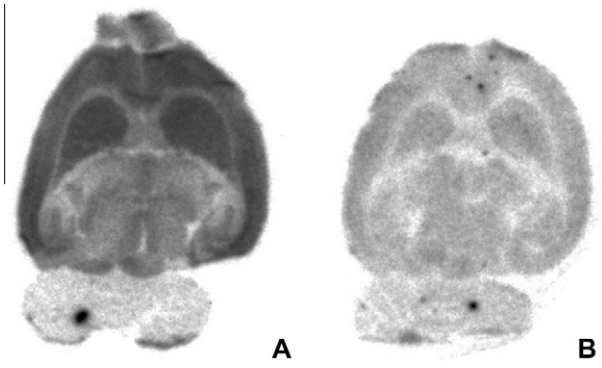

Figure 4. In vitro ^{18}F-ST889 autoradiography of horizontal sections of a rat brain under baseline (A) and blocking (B) conditions (co-incubation with 100 μM histamine).

2.8. PET imaging

Based on the in vitro characterization described above, ^{18}F-ST889 was further evaluated as a potential radiotracer for CNS H_3R imaging in vivo. A whole body scan at 70–100 min post injection (p.i.) revealed that ^{18}F-ST889 or its radiometabolites are cleared mainly via the renal pathway (Fig. 5). Highest activity concentrations were found in the urinary bladder and the kidney pelvis. Hepatobiliary elimination of the tracer was also apparent by activity accumulation in the liver and intestine. Furthermore, the whole body PET image of ^{18}F-ST889 suggested minor defluorination of the parent compound at this late time point since some radioactivity uptake was observed in joints and the skeleton, in particular the spinal column. High ^{18}F-ST889 accumulation was identified in various glandular tissues such as thyroid, adrenals and salivary glands. Noteworthy, high levels of thyroid accumulation were observed with other potential H_3R probes, such as ^{123}I-iodoproxyfan and ^{125}I-WYE-230949, and was attributed to in vivo deiodination of the radiotracer and accumulation of free iodine in the thyroid, which is a known phenomenon.[41,42] This explanation is not applicable in our case. There must be another mechanism of non-specific glandular accumulation of the tracer or its metabolite(s).

No appreciable accumulation of ^{18}F-ST889 could be observed in the H_3R-expressing forebrain areas (striatum and cerebral cortex) (Fig. 6). Only one hot spot was observed within the brain and co-registered CT images suggested that this basally located hot spot most probably corresponds to the pituitary gland. High accumulation of radioactivity was also visible in other secretory tissues such as the Harderian and intraorbital lacrimal glands and salivary gland. Co-administration of the blocking compound, ST900 ($K_i = 0.068$ nM to recombinant human H_3R)[27] (1 mg per kg body weight) or ciproxifan ($K_i = 0.654$ nM to rat cortex H_3R)[43] (2 mg per kg body weight) with ^{18}F-ST889 did not block the signal (Fig. 7) suggesting nonspecific tracer accumulation. Interestingly, radioactivity in other brain regions such as cerebral cortex and cerebellum was slightly elevated under both blocking conditions. Such a phenomenon could result from blocking of peripheral binding sites or metabolizing enzymes resulting in a greater availability

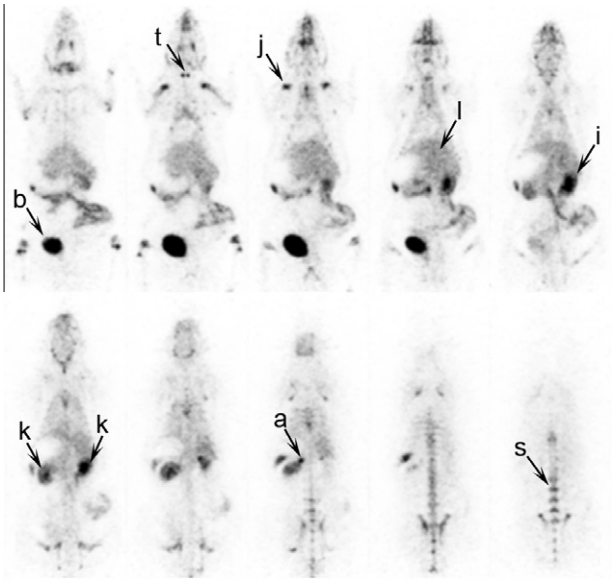

Figure 5. Series of horizontal whole body slices (ventral to dorsal) through a rat injected with ^{18}F-ST889. The images were obtained by reconstructing data from 70 to 100 min after injection (b–urinary bladder, t–thyroid, j–joint, l–liver, i–intestine, k–kidney, a–adrenal, s–spinal column).

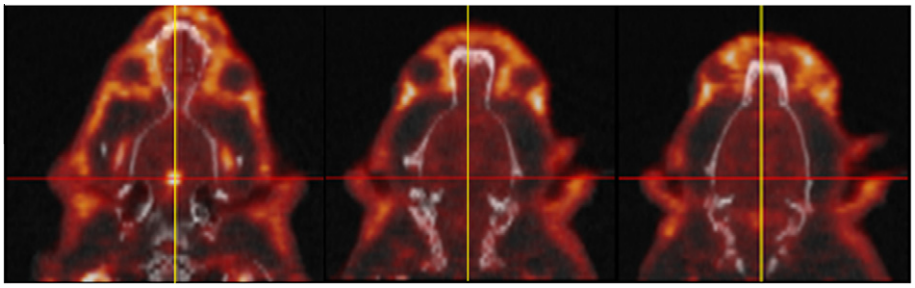

Figure 6. Representative horizontal PET/CT slices through a rat's head injected with ^{18}F-ST889. The images were obtained by reconstructing data from 0 to 60 min after injection (averaged). CT data are given in grey values whereas PET data are shown in color (highest activity concentration: yellow, moderate activity concentration: red).

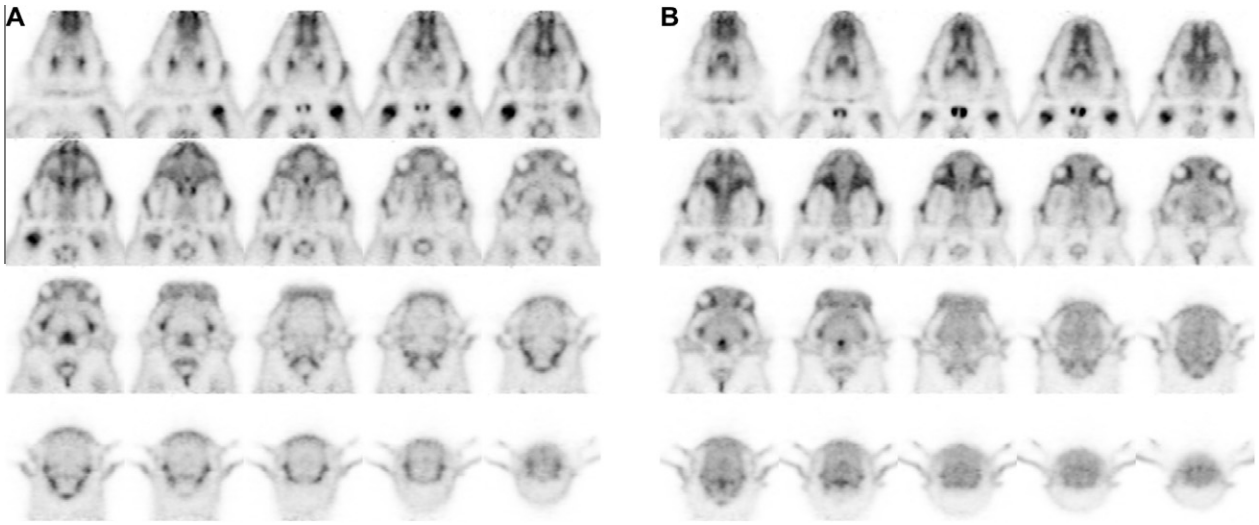

Figure 7. Series of horizontal slices through a rat's head (ventral to dorsal). The animal was injected with ^{18}F-ST889 alone (A, baseline) or co-injected with 2 mg/kg ciproxifan (B). The images were obtained by reconstructing data from 0 to 60 min after injection (averaged).

of the radioligand in blood.[44] Evaluation of the dynamic PET data demonstrated that brain signals reached a plateau within 10 min after tracer injection and were persistent over the 60 min acquisition time without any significant washout. Furthermore, time-activity curves for other organs, in particular glandular tissue, showed stable radioactivity level or even slight increase (data not shown). Taken together, our in vivo data indicate that ^{18}F-ST889 does not bind selectively to H_3R in the rat brain.

2.9. In vivo metabolism

Only intact radiotracer was detected in plasma samples taken at 5, 15, and 30 min after injection. Urine sample taken at 30 min after injection displayed three radioactive compounds, one of them being ^{18}F-ST889, which accounted for 90% of the total radioactivity. Therefore, the tracer stability may not be the reason for the low brain uptake. The radiometabolites (7% and 3%) were more hydrophilic. The radiometabolite eluting with solvent front (7%) may suggest partial defluorination in vivo, which results in visible bone uptake at late imaging time (Fig. 5).

3. Conclusion

We conclude that despite proven specificity of ^{18}F-ST889 in vitro, the compound is not suitable as a PET tracer for brain imaging of H_3R in rats. Most probably it is related to restricted BBB passage due to the moderate lipophilicity and low permeation coefficient. Brain imaging in (non-human) primates could provide for a more suitable trial of the tracer utility for imaging humans. It is worth to mention that three successful imaging studies of H_3R reported previously were performed in rhesus monkeys,[24] pigs,[45] and humans.[25,26]

4. Experimental

All commercial reagents and solvents were used as supplied by Sigma–Aldrich or Merck unless stated otherwise. Reactions were monitored by UPLC. The system was Acquity UPLC from Waters, equipped in addition with a FlowStar LB 513 radiodetector (Berthold Technologies) and a UPLC dedicated reversed-phase Acquity BEH C18, particle size 1.7 μm, 100 × 2.1 mm column. The mobile phase was a gradient of acetonitrile in water with 0.1% trifluoroacetic acid (TFA) from 0% to 100% over 2 min, flow rate of 0.7 mL/min. Analytical HPLC was performed on an Agilent 1100 series system equipped with a Raytest Gabi Star radiodetector. Analytical reversed phase column was Phenomenex Gemini C18, particle size 5 μm, 250 × 4.6 mm. A gradient of acetonitrile in water with 0.1% TFA from 10% to 25% over 12 min, flow rate of 1 mL/min was used. Semipreparative HPLC was carried out on an HPLC system equipped with a Merck-Hitachi L-6200A Intelligent pump, a 5 mL injection loop, a Knauer Variable Wavelength Monitor UV-detector, and an Eberline RM-14 radiodetector on a reversed-phase Phenomenex Gemini C18 column, particle size 5 μm, 250 × 10 mm. The mobile phase consisted of isocratic 10% acetonitrile/90% water with 0.1% TFA v/v, eluted at 4 mL/min flow rate. UV-absorbance was detected at 226 nm. TLC plates were

Macherey-Nagel SIL G-25 UV254 normal phase silica. The mobile phase consisted of acetonitrile/50 mM ammonium bicarbonate buffer pH 8 (3:1). Protein concentrations were determined using Genesys 10 UV Scanning spectrophotometer (Thermo Fischer Scientific).

4.1. ^{18}F-fluoride production

No-carrier-added (n.c.a) ^{18}F-fluoride was produced via the ^{18}O(p,n) ^{18}F nuclear reaction in a fixed-energy Cyclone 18/9 cyclotron (IBA, Belgium). For this >98% isotopically enriched ^{18}O-water (Nukem GmbH, Germany) was irradiated by 18 MeV proton beam. Small volume liquid target (0.5 mL) was used to produce radioactivity for reaction optimization experiments. Large volume liquid target (2.0 mL) was used when labeled compound was produced for biological experiments. Produced ^{18}F-fluoride/^{18}O-water solution was transferred using a helium stream from the target to a shielded hot cell equipped with a manipulator, where radiosynthesis was performed. Typical production of ^{18}F-fluoride at EOB of the 2 mL target for 35 mAh (45 min) was 80–100 GBq.

4.2. Radiosynthesis

Precursor for radiolabeling and cold reference compound were synthesized as described previously.[27]

^{18}F-fluoride (~80–100 GBq) was trapped on an anion exchange Sep-Pak Light Accell Plus QMA cartridge (Waters) preconditioned with 5 mL 0.5 M potassium carbonate solution followed by 10 mL water and flushed with 10 mL air. It was eluted with 1.5 mL solution of Kryptofix 2.2.2 (4,7,13,16,21,24-hexaoxa-1,10-diazabicyclo[8.8.8]-hexacosane) (5 mg) and potassium carbonate (1 mg) in 80% acetonitrile in water. Effluent was collected to a tightly closed 10 mL Reacti-Vial (Thermo Fisher Scientific) and solvent was evaporated under stream of nitrogen and reduced pressure (50–80 mbar) at 100 °C. The residue was azeotropically dried by addition of 3 × 1 mL of dry acetonitrile. Precursor ST-928 (1.97–2.35 mg, 4.8–5.7 μmol) predissolved in 300 μl acetonitrile was added to the dry ^{18}F-Kryptofix complex and the reaction mixture was heated at 100 °C for 30 min. After 5 min of cooling at room temperature 4 mL of 0.1% TFA solution in water (v/v) was added to the vial and injected into semi-preparative HPLC at once (for conditions see Section 4). The radioactive fraction eluting at t_R = 17–18 min was collected and radio-fluorinated product was concentrated using solid phase extraction. For this, the collected solution was diluted with 10 mL water for injection and passed through Sep-Pak Light C18 cartridge (preconditioned in advance with 5 mL ethanol followed by 10 mL H_2O). Cartridge was washed with additional 10 mL water for injection and ^{18}F-ST889 was eluted with 0.5 mL ethanol to a penicillin vial. Ethanol fraction was diluted with 9.5 mL PBS and passed through a 13 mm Nalgene 0.2 μm sterile filter (Thermo Fisher Scientific) to a sterile vial, giving an injectable sterile solution containing 5% ethanol by volume, which was used for biological experiments.

4.3. Quality control

An aliquot of known volume and radioactivity of the final formulated solution was injected into analytical HPLC for quality control, which required approximately 15 min (for conditions see Section 4). The retention time of the radiolabeled product was 10.7 min. and the formulation contained no precursor (expected t_R = 11.5 min). The specific radioactivity was determined from the quality control run matching the area of the UV absorbance peak at 226 nm, which co-eluted with the radiolabeled product, to a standard calibration curve calculated using known concentrations of the non-radioactive reference compound.

4.4. Preparation of crude rat brain membranes

The rats (Sprague–Dawley, 7–8 weeks old, mixed gender) were sacrificed by decapitation. The brains were removed, separated from the cerebellum and homogenized (Polytron PT-2100, Kinematica) in 10 volumes of ice-cold 10 mM Tris/acetate buffer pH 7.4 containing sucrose (0.32 M) for 1 min at setting 4. After centrifugation (1000×*g*, 15 min, 4 °C) the supernatant containing the membranes was collected and kept aside. The pellet was resuspended in five volumes of Tris buffer (as above) and the homogenizing procedure was repeated. The pellet was discarded and the supernatants were combined and centrifuged at 17000×*g* for 20 min at 4 °C to precipitate the membranes. The supernatant was decanted; the pellet was resuspended in 5 mM Tris/acetate buffer pH 7 and centrifuged again (17000×*g*, 20 min, 4 °C). This last procedure was repeated three times. The final pellet was reconstituted in 5 mM Tris/acetate buffer pH 7.4, stored in aliquots at −80 °C, and thawed on the day of the experiment. Protein content was determined by Bradford assay using bovine serum albumin as standard protein.[46]

4.5. Binding affinity to rat H_3R

The binding assay was performed with 6×10^{-11} M ^{18}F-ST889 (specific radioactivity 52 GBq/μmol at EOS) alone or in combination with cold ST889 at 10 different concentrations, ranging from 3×10^{-11} M to 10^{-5} M in a final volume of 0.2 mL (3 samples per concentration). Nonspecific binding was estimated in the presence of 10 μM (*R*)-α-methylhistamine, an established selective H_3R ligand. The membranes (75 μg/mL protein) were incubated together with above mentioned compounds in HEPES buffer (30 mM sodium 4-(2-hydroxyethyl)-1-piperazineethanesulfonate (Na-HEPES), 110 mM NaCl, 5 mM KCl, 2.5 mM $CaCl_2$, and 1.3 mM $MgCl_2$, pH 7.4) for 1 h at room temperature. The incubation was terminated by addition of ice cold HEPES buffer and rapid filtration through glass microfiber GF/B grade filters (Whatman) presoaked in 0.05% polyethylenimine (Fluka). The filters were washed three times with 4 mL ice-cold HEPES buffer and radioactivity trapped on the filters was counted in an automatic gamma counter (Wallac 1480 Wizard 3″, Perkin Elmer). K_d and B_{max} values were estimated using (Eq. 1) by non-linear curve fitting in Excel (MS Office 2007, Microsoft):

$$B = \frac{B_{max,1} \times K_{a,1} \times ([ST889_{total}] - [ST889_{bound}])}{1 + K_{a,1} \times ([ST889_{total}] - [ST889_{bound}])} + \frac{B_{max,2} \times K_{a,2} \times ([ST889_{total}] - [ST889_{bound}])}{1 + K_{a,2} \times ([ST889_{total}] - [ST889_{bound}])} \quad (1)$$

The parameter B indicates the quantity of ST889 bound in mol/mg protein; B_{max} is the maximal binding capacity in mol/mg protein. K_a is the association constant, that is, $1/K_d$, in M^{-1}. $[ST889_{total}]$ and $[ST889_{bound}]$ are the total and bound molar concentrations of ST889 in the incubation mixture, respectively. The bound concentration was calculated from the amount trapped on the filter and the sample volume. The estimated binding parameters were confirmed by Scatchard plot, that is, $B/([ST889_{total}]-[ST889_{bound}])$ versus B.

4.6. Lipophilicity determination ($\log D_{7.4}$)

Lipophilicity was determined using the shake-flask method[33] by partitioning the radiolabeled compound between 1-octanol and aqueous phosphate buffer solution at pH 7.4. Both solvents were pre-saturated with each other. First, octanol (2 mL), saturated with buffer, aqueous phosphate buffer (2 mL), saturated with octanol, and formulated ^{18}F-ST889 solution (50 μl) were mixed in a separation funnel. After phase separation the aqueous phase was

discarded to remove any possible polar impurities. Next, the purified octanol phase (300 μl), containing the radiotracer (~700 kBq), and fresh phosphate buffer at pH 7.4 (300 μl), saturated with octanol, were mixed in three Eppendorf microcentrifuge tubes. The Eppendorf tubes were tightly closed and rotated on an upside-down shaker for 30 min. The phases were separated by 20 min centrifugation at 6700×*g*. An aliquot (30 μl) of both phases from each Eppendorf tube was removed and the radioactivity of these samples was counted in a gamma counter. The distribution coefficient $D_{7.4}$ was calculated dividing the averaged radioactivity concentration in the octanol phase by the averaged radioactivity concentration in the aqueous phase. The reported $\log D_{7.4}$ is the mean of three independent determinations.

4.7. In vitro plasma stability

Human or rodent plasma was centrifuged at room temperature at 270×*g* for 10 min. An aliquot of 50 μl (~60 MBq) of radiolabeled compound solution was added to the plasma supernatant (~0.5 mL) and vortexed. The resulting plasma containing ^{18}F-ST889 was distributed into six Eppendorf microcentrifuge tubes, 70 μl (~7 MBq) to each. The first tube, which represented zero time point, already contained 70 μl methanol. Five other tubes were incubated at 37 °C in an Eppendorf Thermomixer Compact (VaudauxEppendorf). The samples were quenched with 70 μl methanol, one by one, after 5, 30, 60, 90, and 120 min. Precipitated plasma proteins were removed by centrifugation at 6700×*g* for 10 min. The supernatants were injected into UPLC for analysis.

4.8. In vitro stability in liver microsomes

Human and rat liver microsomes were purchased from BD Biosciences as 20 mg protein/mL solution and stored at −80 °C. They were thawed before use and stored on ice. The general assay procedure suggested by the supplier was optimized for our use. Formulated ^{18}F-ST889 (100 μl, ~5 MBq), reduced nicotinamide adenine dinucleotide phosphate (NADPH) (100 μl of 10 mM solution), and PBS (775 μl of 0.15 M solution) were added to an Eppendorf microcentrifuge tube. The mixture was incubated at 37 °C for 5 min. The enzymatic reaction was initiated by addition of 25 μl of human or rat liver microsomes. Hundred microliter of this solution was withdrawn right away and quenched with 100 μl of ice-cold acetonitrile to represent zero time point. The mixture was then incubated for additional 120 min. Samples (100 μl) of the incubating solution were transferred into a different Eppendorf tube and quenched with 100 μl of ice-cold acetonitrile at 15, 30, 60, and 120 min. The samples were vortexed and centrifuged at 6700×*g* for 3 min. The supernatants (50 μl) were transferred into HPLC vials and analyzed by UPLC. Testosterone (100 μl of 0.5 mM solution, final concentration 50 μM) was used instead of ^{18}F-ST889 as a positive control. A mixture of testosterone (100 μl of 0.5 mM solution) and PBS (900 μl of 0.15 M solution) without microsomes was incubated along with other samples and served as a negative control and to determine initial area under UV peak for testosterone. UV absorption for the testosterone was measured at 245 nm.

4.9. In vitro autoradiography

Whole brain horizontal slices (20 μm) of a male Sprague Dawley rat mounted on SuperFrost microscope adhesion slides (MenzelThermo Fisher Scientific) were thawed for 30 min and incubated for 45 min with a 0.01 nM solution of ^{18}F-ST889 in PBS containing 5% ethanol (v/v) at room temperature. Nonspecific binding was determined in the presence of 100 μM histamine. The slices were washed three times for 3 min in PBS at 4 °C and twice for 5 s in distilled water and then air dried for 20 min at rt. The sections were placed in a light-tight cassette and exposed to a BAS-TR 2025 phosphor imaging plate (RaytestFuji). After 15 min exposure time the imaging plates were scanned in a BAS-5000 bio-imaging analyzer with a resolution of 50 μm (Fujifilm). Data were analyzed and processed with the AIDA 2.31 software (RaytestFuji).

4.10. In vitro P-gp transport

Madin–Darby canine kidney cells strain II transfected with human P-glycoprotein (MDCKII-*h*MDR1) were provided by the Netherlands Cancer Institute (Amsterdam, Netherlands). Cells were cultured in Dulbecco's modified Eagle medium (DMEM) containing GlutaMAX (Gibco, Invitrogen), 100 U/mL penicillin/100 μg/mL streptomycin mixture (Invitrogen), and 10% fetal bovine serum (Invitrogen) and were split 1:5 twice weekly. For transport studies the cells were seeded into 4.2 cm^2, 0.4 μm BD Falcon polyethylene terephthalate culture inserts (BD Biosciences) at a density of 500,000 cells/cm^2. Culture medium (3 mL) on the apical (insert) and basal (well) sides was replaced daily. Transport experiments were performed 3 days after the seeding. The medium was replaced by DMEM containing 10 mM HEPES and 1% fetal calf serum, and 400 kBq ^{18}F-ST889 (formulated in PBS containing 5% ethanol) or 20 kBq ^{3}H-vinblastine (2.96 GBq/mmol, Perkin Elmer), a known P-glycoprotein substrate, were added either to the apical or the basal compartment (donor compartments). The cultures were incubated at 37 °C on a rocking plate and 100 μl samples were withdrawn from the acceptor compartments after 20, 40, 60 and from both the acceptor and donor compartments after 80 min. ^{18}F-ST889 and ^{3}H-vinblastine were quantified with a gamma counter and a LS6500 liquid scintillation counter (Beckman Coulter), respectively. The experiments were repeated in the presence of verapamil hydrochloride (10 μM and 100 μM) and elacridar (10 μM) to inhibit P-gp function. Permeation coefficients (P_{app}) were calculated according to (Eq. 2):

$$P_{app} = \frac{1}{A \times C_0} \times \frac{\Delta Q_r}{\Delta t} \quad (2)$$

where A is the area of the cell layer (4.2 cm^2), C_0 is the initial compound concentration (mol/cm^3) in the donor compartment, and ΔQ_r is the quantity (mol) of compound transported to the acceptor compartment over the period of time Δt (sec). A ratio P_{app} (B→A)/P_{app} (A→B) >1 in the absence of a P-gp inhibitor indicates that compound is a P-gp substrate.

4.11. In vivo PET imaging

Animal care and all experimental procedures were approved by the Veterinary Office of the Canton Zurich. Adult male Sprague–Dawley rats were obtained from Charles River (Germany) and were allowed free access to food and water. For PET scanning rats were immobilized by an isoflurane inhalation anesthesia using an oxygen/air mixture as carrier gas. Monitoring of anesthesia was performed according to protocols published previously.[47] In the first PET experiment, a rat was scanned in a whole body configuration to obtain data on whole body distribution of ^{18}F-ST889 and the main elimination pathways. For this purpose, a rat (475 g) was injected with 29.1 MBq (0.33 nmol) of the tracer and scanned in the quad-HIDAC PET tomograph (Oxford Positron Systems, UK) during 70–100 min post injection in a single bed position. Acquired data were reconstructed in a single time frame with a bin size of 1.0 mm and a matrix size of 250 × 100 × 100 mm. In a second set of PET experiments, the heads of four rats were scanned in the GE VISTA PET/CT tomograph, which is characterized by high sensitivity but a limited axial field-of-view of 4.8 cm.[48] Animals were anesthetized and fixed on the bed of the tomograph before

tracer injection. Two animals were injected into a tail vein with ^{18}F-ST889 alone (injected dose 29–44 MBq; injected mass 0.27–0.33 nmol), one animal was co-injected with the blocker ST900 (1 mg per kg body weight), and another animal was co-injected with the blocker ciproxifan (2 mg per kg body weight). All animals were scanned for 0–60 min after tracer injection in a dynamic PET acquisition mode. After the PET scan one animal was subjected to a CT scan to obtain fused PET/CT images for a better anatomical assignment of radioactive signals. Raw data were acquired in list-mode and reconstructed in user-defined time frames (dynamic: 5×2, 6×5, 2×10 min; static: 1×60 min) with a voxel size of $0.3875 \times 0.3875 \times 0.775$ mm and a matrix size of $175 \times 175 \times 61$. Image files were evaluated by ROI analysis using the dedicated PMOD software.[49] Time-activity curves were normalized to the injected dose per gram of body weight and expressed as standardized uptake values (SUV).

4.12. In vivo metabolism

A rat was injected with ~250 MBq (~7 nmol, 300 μL) of the tracer via a lateral tail vein. Blood samples were withdrawn at 5 and 15 min after injection. The animal was sacrificed at 30 min after injection and blood and urine was collected. The samples were placed into 1.5 ml Eppendorf microcentrifuge tubes and centrifuged (5000×*g*, 5 min, 4 °C). The supernatants were decanted into separate Eppendorf tubes and the proteins were precipitated by addition of an equal volume of ice-cold methanol. The tubes were centrifuged (5000×*g*, 5 min, 4 °C). The supernatants were transferred into HPLC vials and analyzed by UPLC and TLC (see conditions in Section 4).

Acknowledgments

We thank Claudia Keller for the excellent technical help in conducting in vitro and in vivo experiments. Support from the COST Action BM0806 for K.I. and H.S. is acknowledged.

References and notes

1. Tiligada, E.; Zampeli, E.; Sander, K.; Stark, H. Expert Opin. Investig *Drugs* **2009**, *18*, 1519.
2. Oda, T.; Morikawa, N.; Saito, Y.; Masuho, Y.; Matsumoto, S. *J. Biol. Chem.* **2000**, *275*, 36781.
3. Thurmond, R. L.; Desai, P. J.; Dunford, P. J.; Fung-Leung, W.-P.; Hofstra, C. L.; Jiang, W.; Nguyen, S.; Riley, J. P.; Sun, S.; Williams, K. N.; Edwards, J. P.; Karlsson, L. *J. Pharmacol. Exp. Ther.* **2004**, *309*, 404.
4. Haas, H.; Panula, P. Nature Rev. *Neuroscience* **2003**, *4*, 121.
5. Leurs, R.; Bakker, R. A.; Timmerman, H.; de Esch, I. J. P. *Nature Rev. Drug Discov.* **2005**, *4*, 107.
6. Passani, M. B.; Lin, J. S.; Hancock, A.; Crochet, S.; Blandina, P. *Trends Pharmacol. Sci.* **2004**, *25*, 618.
7. Gemkow, M. J.; Davenport, A. J.; Harich, S.; Ellenbroek, B. A.; Cesura, A.; Hallett, D. *Drug Discov. Today* **2009**, *14*, 509.
8. Lovenberg, T. W.; Roland, B. L.; Wilson, S. J.; Jiang, X.; Pyati, J.; Huvar, A.; Jackson, M. R.; Erlander, M. G. *Mol. Pharmacol.* **1999**, *55*, 1101.
9. Wijtmans, M.; Leurs, R.; de Esch, I. Expert Opin. Investig *Drugs* **2007**, *16*, 967.
10. Arrang, J. M.; Garbarg, M.; Schwartz, J. C. *Nature* **1983**, *302*, 832.
11. Schwartz, J. C.; Arrang, J. M.; Garbarg, M.; Pollard, H.; Ruat, M. *Physiol. Rev.* **1991**, *71*, 1.
12. Leurs, R.; Smit, M. J.; Timmerman, H. *Pharmacol. Therapeut.* **1995**, *66*, 413.
13. Sander, K.; Kottke, T.; Stark, H. *Biol. Pharm. Bull.* **2008**, *31*, 2163.
14. Cumming, P.; Shaw, C.; Vincent, S. R. *Synapse* **1991**, *8*, 144.
15. Pollard, H.; Moreau, J.; Arrang, J. M.; Schwartz, J. C. *Neuroscience* **1993**, *52*, 169.
16. Ponchant, M.; Demphel, S.; Fuseau, C.; Coulomb, C.; Bottlaender, M.; Schwartz, J. C.; Stark, H.; Schunack, W.; Athmani, S.; Ganellin, R.; Crouzel, C. Symposium abstract, XII International Symposium on Radiopharmaceutical Chemistry, Uppsala, Sweden, June 15-19, 1997; *J. Label. Compd. Radiopharm.* **1997**, *40*, 605.
17. Windhorst, A. D.; Timmerman, H.; Menge, W. M. P. B.; Leurs, R.; Herscheid, J. D. M. J. *Label. Compd. Radiopharm.* **1999**, *42*, 293.
18. Windhorst, A. D.; Timmerman, H.; Klok, R. P.; Menge, W. M. P. B.; Leurs, R.; Herscheid, J. D. M. *Bioorg. Med. Chem.* **1999**, *7*, 1761.
19. Iwata, R.; Horváth, G.; Pascali, C.; Bogni, A.; Yanai, K.; Kovacs, Z.; Ido, T. *J. Label. Compd. Radiopharm.* **2000**, *43*, 873.
20. Funaki, Y.; Sato, K.; Kato, M.; Ishikawa, Y.; Iwata, R.; Yanai, K. *Nucl. Med. Biol.* **2007**, *34*, 981.
21. Yang, R.; Hey, J. A.; Aslanian, R.; Rizzo, C. A. *Pharmacology* **2002**, *66*, 128.
22. Airaksinen, A. J.; Jablonowski, J. A.; van der Mey, M.; Barbier, A. J.; Klok, R. P.; Verbeek, J.; Schuit, R.; Herscheid, J. D. M.; Leysen, J. E.; Carruthersb, N. E.; Lammertsmaa, A. A.; Windhorst, A. D. *Nucl. Med. Biol.* **2006**, *33*, 801.
23. Hamill, T. G.; Sato, N.; Jitsuoka, M.; Tokita, S.; Krause, S.; Ryan, C.; Gantert, L.; Sleph, H.; Zeng, Z.; Miller, P.; Patel, S.; Riffel, K.; Sanabria, S.; Eng, W.; Chen, T.; Renger, J. J.; Doran, S.; Garson, S.; Iannone, R.; Hargreaves, R.; Burns H. D. Abstracts of Papers, 7th International Symposium on Functional Neuroreceptor Mapping of the Living Brain, Pittsburgh, PA, July 17-19, 2008; NeuroImage 2008, 41, T22.
24. Hamill, T. G.; Sato, N.; Jitsuoka, M.; Tokita, S.; Sanabria, S.; Eng, W.; Ryan, C.; Krause, S.; Takenaga, N.; Patel, S.; Zeng, Z.; Williams, D., Jr.; Sur, C.; Hargreaves, R.; Burns, H. D. *Synapse* **2009**, *63*, 1122.
25. Ashworth, S.; Cunningham, V.; Rabiner, E.; Lai, R.; Sivananthan, T.; Plisson, C.; Wilson, A.; Comley, R.; Gee A.; Laruelle M. Abstracts of Papers, Society of Nuclear Medicine Annual Meeting, New Orleans, LA, June 14–18, 2008; *J. Nucl. Med.* **2008**; *49*(Supplement 1), 210P.
26. Ashworth, S.; Rabiner, E. A.; Gunn, R. N.; Plisson, C.; Wilson, A. A.; Comley, R. A.; Lai, R. Y. K.; Gee, A. D.; Laruelle, M.; Cunningham, V. J. *J. Nucl. Med.* **2010**, *1021*, 51.
27. Isensee, K.; Amon, M.; Galaparti, A.; Ligneau, X.; Camelin, J.-C.; Capet, M.; Schwartz, J.-C.; Stark, H. *Bioorg. Med. Chem. Lett.* **2009**, *19*, 2172.
28. Apodaca, R.; Dvorak, C. A.; Xiao, W.; Barbier, A. J.; Boggs, J. D.; Wilson, S. J.; Lovenberg, T. W.; Carruthers, N. I. *J. Med. Chem.* **2003**, *46*, 3938.
29. Barbier, A. J.; Berridge, C.; Dugovic, C.; Laposky, A. D.; Wilson, S. J.; Boggs, J.; Aluisio, L.; Lord, B.; Mazur, C.; Pudiak, C. M.; Langlois, X.; Xiao, W.; Apodaca, R.; Carruthers, N. I.; Lovenberg, T. W. *Brit. J. Pharmacol.* **2004**, *143*, 649.
30. Miko, T.; Ligneau, X.; Pertz, H. H.; Ganellin, R. C.; Arrang, J. M.; Schwartz, J. C.; Schunack, W.; Stark, H. *J. Med. Chem.* **2003**, *46*, 1523.
31. Scott, P. J. H.; Hockley, B. G.; Kung, H. F.; Manchanda, R.; Zhang, W.; Kilbourn, M. R. *Appl. Radiat. Isotopes* **2009**, *67*, 88.
32. ter Laak, A. M.; Tsai, R. S.; Denkelder, G. M. D. O.; Carrupt, P. A.; Testa, B.; Timmerman, H. *Eur. J. Pharm. Sci.* **1994**, *2*, 373.
33. Wilson, A. A.; Jin, L.; Garcia, A.; DaSilva, J. N.; Houle, S. *Appl. Radiat. Isotopes* **2001**, *54*, 203.
34. Waterhouse, R. N. *Mol. Imaging Biol.* **2003**, *14*, 376.
35. Pike, V. W. *Trends Pharmacol. Sci.* **2009**, *30*, 431.
36. Hagmann, W. K. *J. Med. Chem.* **2008**, *51*, 4359.
37. Sun, S.; Adejare, A. *Curr. Top. Med. Chem.* **2006**, *6*, 1457.
38. Didziapetris, R.; Japertas, P.; Avdeef, A.; Petrauskas, A. J. *Drug Target* **2003**, *11*, 391.
39. Mahar Doan, K. M.; Humphreys, J. E.; Webster, L. O.; Wring, S. A.; Shampine, L. J.; Serabjit-Singh, C. J.; Adkison, K. K.; Polli, J. W. *J. Pharmacol. Exp. Ther.* **2002**, *303*, 1029.
40. Nagase, T.; Mizutani, T.; Ishikawa, S.; Sekino, E.; Sasaki, T.; Fujimura, T.; Ito, S.; Mitobe, Y.; Miyamoto, Y.; Yoshimoto, R.; Tanaka, T.; Ishihara, A.; Takenaga, N.; Tokita, S.; Fukami, T.; Sato, N. *J. Med. Chem.* **2008**, *51*, 4780.
41. Ligneau, X.; Lin, J.-S.; Vanni-Mercier, G.; Jouvet, M.; Muir, J. L.; Ganellin, C. R.; Stark, H.; Elz, S.; Schunack, W.; Schwartz, J. C. J. *Pharmacol. Exp. Ther.* **1998**, *287*, 658.
42. Briard, E.; Zoghbi, S. S.; Imaizumi, M.; Gourley, J. P.; Shetty, H. U.; Hong, J.; Cropley, V.; Fujita, M.; Innis, R. B.; Pike, V. W. *J. Med. Chem.* **2008**, *51*, 17.
43. Windhorst, A. D.; Timmerman, H.; Klok, R. P.; Custers, F. G. J.; Menge, W. M. P. B.; Leurs, R.; Stark, H.; Schunack, W.; Gielen, E. G. J.; van Kroonenburgh, M. J. P. G.; Herscheid, J. D. M. *Nucl. Med. Biol.* **1999**, *26*, 651.
44. Lewis, D. Y.; Champion, S.; Dewar, D.; Honey, G.; Gross, J.; Robichaud, A. J.; Welch, A.; Wyper, D.; Pimlott, S. *Abstracts of Papers*; World Molecular Imaging Congress: Montreal, Canada, 2009. September 23–26.
45. Plisson, C.; Gunn, R. N.; Cunningham, V. J.; Bender, D.; Salinas, C. A.; Medhurst, A. D.; Roberts, J. C.; Laruelle, M.; Gee, A. D. *J. Nucl. Med.* **2009**, *50*, 2064.
46. Bradford, M. M. *Anal. Biochem.* **1976**, *72*, 248.
47. Honer, M.; Brühlmeier, M.; Missimer, J.; Schubiger, A. P.; Ametamey, S. M. *J. Nucl. Med.* **2004**, *45*, 464.
48. Wang, Y.; Seidel, J.; Tsui, B. M. W.; Vaquero, J. J.; Pomper, M. G. *J. Nucl. Med.* **1891**, *2006*, 47.
49. Mikolajczyk, K.; Szabatin, M.; Rudnicki, P.; Grodzki, M.; Burger, C. *Med. Inform.* **1998**, *23*, 207.